



Trade Science Inc.

Nano Science and Nano Technology

An Indian Journal

Full Paper

NSNTAJ, 4(2), 2010 [77-85]

Optical properties of anisotropic nanogolds from finite element method

M.Benhamou^{1*}, A.R.Senoudi², F.Lallam², A.Boussaid², A.Bensafi²

¹Polymer Physics and Critical Phenomena Laboratory, Sciences Faculty Ben M'sik,
P.O.Box 7955, Casablanca, (MOROCCO)

²Physics Department, Sciences Faculty, Abou Bekr Belkaid University, 13000-Tlemcen, P.O.Box 119, (ALGERIA)

E-mail : benhamou.mabrouk@gmail.com

Received: 9th July, 2010 ; Accepted: 19th July, 2010

ABSTRACT

In this paper, we consider dispersed nanogolds, and the aim is a quantitative study of the associated optical absorption and scattering cross-sections, as a function of their shape and aspect ratio. The finite element method, known to be a very useful and versatile computational tool for particles with any arbitrary shape and embedded in a dielectric matrix, is used. Our study is focused on the ellipsoid and cylinder shapes. The obtained numerical results are naturally compared to those predicted by theoretical models. Also, we discuss the effects of the shell on the cylinder plasmonic behaviors. The main conclusion is that, the shape is another pertinent parameter that drastically affects the optical properties of the dispersed nanogolds. © 2010 Trade Science Inc. - INDIA

KEYWORDS

Nanogolds;
Optical cross-section;
Polarization;
Shell;
Finite element method.

INTRODUCTION

Gold nanoellipsoids and nanorods exhibit transverse and longitudinal surface plasmon resonance (LSP) in infrared band. At normal incidence or with s-polarized light, where the incident electric field vibrates perpendicularly to the ellipsoid long-axis, the spectra reveal one single peak at around 520nm wavelength. This resonance is associated with transverse (T) plasmonic excitation in the direction normal to the ellipsoid long-axes^[1,2]. At oblique incidence and with p-polarized light, where the incident electric field has a component both along and perpendicular to the ellipsoid long-axes, the spectra present two peaks : the above-mentioned T mode as well as a longer-wavelength resonance, the L mode associated with a plasmonic excitation polarized

along the ellipsoid long-axes, and this latter mode occurs at around 700nm. The L-mode resonance wavelength is strongly dependent on both ellipsoid aspect ratio and the distance between the inclusions in the host matrix. In accordance with the dipolar plasmonic response of ellipsoid, an increase in the aspect ratio causes two resonances to split further apart spectrally, with the T mode undergoing a blue-shift, while the L mode moves towards longer wavelengths^[3].

These nanoparticles are unique, because of its intriguing optical properties that can be exploited for both imaging and therapeutic applications. Also, the resonance light-scattering is of growing interest for particles characterization and biomedical applications. This makes that the gold nanoparticles constitute a very attractive platform for cancer diagnosis and therapy. In

Full Paper

the vicinity of the desired site, the gold nanoparticles are activated through the absorption of radiation of an appropriate wavelength. This strongly absorbed radiation is converted than efficiently into heat on a picosecond time domain, by electron-phonon and phonon-phonon processes^[4-7].

On the other hand, these nanoparticles are of great interest owing to their unique optical properties, including additional localized surface plasmon resonance extinction band which is red shifted, with respect to the short wave-length peaks of spherical particles. Furthermore, they exhibit inherent plasmonic resonance similar to those artificial materials at microwaves. Such extraordinary characteristics enable us to obtain negative permittivity from material as gold. It is so great interesting to know their optical properties.

Mixing rules, for discrete scatters immersed in a host medium, functions of physical properties of the material, volume fraction and spatial arrangement of inclusions, have been recently proposed. It is very common to use the effective medium theory to characterize this kind of media. This representation is often based on the assumption that the inclusions in the medium have sizes and periodicities that are sufficiently small in comparison to the wavelength of the impinging radiation. Under this condition, the composite can be considered as a homogeneous material. The most popular models are the effective medium theory (EMT), the Maxwell Garnett theory (MGT)^[8] and the Bruggeman theory (BT)^[9]. Except at low filling factors (less than 0.1), the two effective medium theories predict strongly different absorption spectra. The MGT is likely to yield better results for metallic inclusions embedded in a dielectric matrix, when there is a sharp interface between the two materials. The BT blurs the sharp interface, and this will broaden the surface plasmon resonance, probably too much at small fractions. In addition, this theory presents the advantage of applicability for arbitrary filling factor, and correctly predicts a percolation threshold to metallic conduction^[10]. It may well yield better results for nanocomposites of less regularly shaped particles or aggregates. However, a classical effective medium analysis neglects the correlations between inclusions that become significant as their concentration increases. These theories often claimed that a weak particle interaction is a condition for the validity of EMT and all the

inclusions are assumed to be spherical.

The optical response of metal nanoparticles to an electromagnetic field of light, for a homogeneous isotropic sphere, was first analytically described by Mie^[11]. On the other hand, for non-spherical particles, approximate numerical methods are generally required, and in recent decades, there are several computational approaches that have been developed, which are based on more advanced scattering theories. These include the T-matrix method^[12], the discrete dipole approximation^[13], and the finite different time domain method^[14].

In this paper, we introduce the Finite Element Method (FEM)^[15,16], which is designed to solve the relevant field equation in the computational domain, subject to the boundary constraints imposed by the geometry. Without making a priori assumption about which field interaction are most significant, numerical techniques analyze the entire geometry provided as input. The FEM, which is a powerful numerical modeling technique, has been widely used for modeling electromagnetic wave interaction with complex materials.

The FEM can provide a full range of plasmon-related properties, including extinction, scattering and absorption cross-sections, and local electric fields, some of which are difficult to measure experimentally. The computer simulation model, based on the FEM we develop, can be applied to two or three-dimensional systems, with two components or more. Within this approach, the FEM is applied, to compute the potential distribution in the composite material and to derive the stored electrical energy, the macroscopic polarization and the absorption and diffusion sections.

This paper is organized as follows. In Sec. II, we review some works dealing with the calculation of the optical properties of anisotropic inclusion embedded in a dielectric matrix. The dispersive function of gold is given dielectric dispersion of gold. In numerical computation, we develop the numerical evaluation, carried out on the composite media, and present the FEM formulation for the resolution of Laplace's equation and formulae for calculating the optical properties of ellipsoid shape. We compare the results obtained for the ellipsoid shape to those provided by literature. In this section, we also present the results relative to the cylinder shape and the shell effect on the LSP. Finally, some concluding remarks are drawn in the last section.

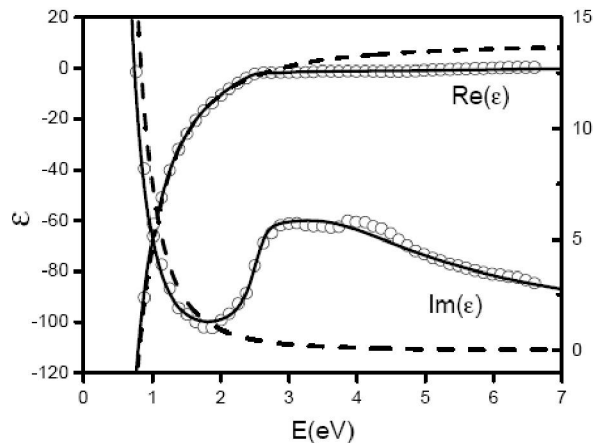


Figure 1 : Real and imaginary parts of the complex gold dielectric function upon energy photon, starting from DCP model (solid line), which was chosen in our calculation. Drude model (dashed line) and measurements (○) are also represented^[23]

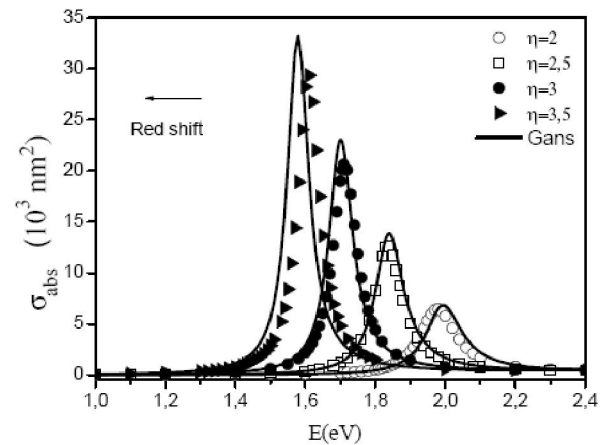


Figure 2 : Absorption cross-section versus photon energy relative to gold prolate shape for longitudinal mode. The symbols (○, □, ● and ▶) represent the numerical results for h 2, 2.5, 3, 3.5, respectively, whereas the solid line describes the analytical ones. The curves are plotted choosing: $2a=20\text{nm}$, $\epsilon_s=2.25$, and $f=0.1$

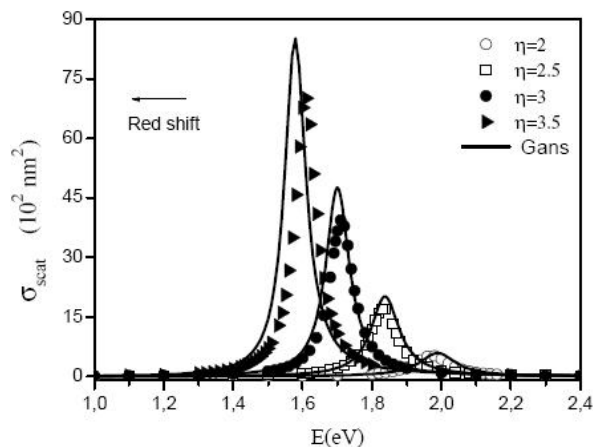


Figure 3 : Absorption cross-section versus photon energy relative to gold prolate shape for longitudinal mode. The symbols (○, □, ● and ▶) represent the numerical results for h 2, 2.5, 3, 3.5, respectively, whereas the solid line describes the analytical ones. In plotting the curves, the numerical parameters are identical to those used in figure 2

Quasi-Static approximation

Generally, the inclusions dimensions are small comparatively to the incident light wave-length. The dipolar approximation is a useful method for computing the optical cross-sections, starting from the polarizability of the metal inclusion.

The present work deals with a composite medium formed by ellipsoidal or cylinder gold inclusions of volume density N , which are dispersed in a host dielectric matrix. We assume that all inclusions have equal masses

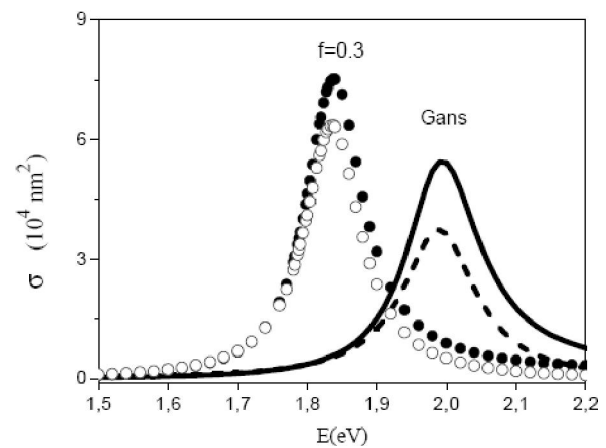


Figure 4 : The symbols (● and ○), corresponding to FEM simulation, represent the absorption and the diffusion, respectively, for $f=0.3$, in the case of the prolate. The analytical results given by the Gans formula correspond to the absorption (solid line) and the diffusion (dashed line). The numerical parameters are as follows: $2a=40\text{nm}$, $2b=80\text{nm}$ and $\epsilon_m=2.25$

and volumes. The filling factor occupied by inclusions is denoted f .

We are interested in two particular shapes, which are the prolate (cigar-shaped) ellipsoid with rotation symmetry, and the cylinder with diameter $2a$ and height $2b$. The prolate ellipsoid is generated by rotating an ellipse around its major axis, which has semi-major axis b and semi-minor axis $a=c$. The gold ellipsoids and the surrounding medium have dielectric functions $\epsilon = \epsilon_1 + \epsilon_2$ and ϵ_m , respectively. In our study, the gold spheroids

Full Paper

are illuminated by polarized light of wave-length k , which is in the direction with an included angle θ makes with z-axis or with x-axis. In the calculation, the size of gold spheroids is much smaller than the wave-length of the incident light. The gold spheroids are then subjected to a uniform static electric field \vec{E} .

When the applied field is arbitrary directed, the induced electric dipole moment^[17] writes as follows,

$$\vec{p} = \epsilon_0 \epsilon_m \left(\alpha_x E_x \vec{u}_x + \alpha_y E_y \vec{u}_y + \alpha_z E_z \vec{u}_z \right) \quad (1)$$

where ϵ_0 is the permittivity of the vacuum, α_x , α_y and α_z are the elements of the polarizability tensor of an individual dipole, whereas the quantities E_x , E_y and E_z stand for the components of the applied field, relative to the principal axes of an anisotropic dipole. Elsewhere, the macroscopic polarization, induced in each metal inclusion of volume V_p , is assumed to be a linear isotropic function and given by,

$$\vec{P} = \frac{\vec{p}}{V_p} \quad (2)$$

The extinction, s_{ext} , the scattering, σ_{scat} , and the absorption, σ_{abs} , cross-sections for small particles, corresponding to the L mode ($\theta=0$), are evaluated using optical theorems^[18].

$$\sigma_{ext} = k \text{Im}(\alpha_z) \quad (3)$$

$$\sigma_{scat} = \frac{k^4 |\alpha_z|^2}{6\pi} \quad (4)$$

$$\sigma_{ext} = \sigma_{scat} + \sigma_{abs} \quad (5)$$

Here, $k = \sqrt{\epsilon_m} k_0$, where k_0 represents the wave-vector of the applied field in the vacuum.

If the incorporated inclusions are physically identical, the total extinction is directly proportional to the inclusion volume density, according to the relation.

$$C_{ext} = N \sigma_{ext} \quad (6)$$

In what follows, we shall compute the optical cross-sections making use of eq. (3-5). To do this, it would be necessary to know the inclusion's polarizability. In facts, different approaches are proposed^[19]; the Clausius-Mossotti relation is generally used^[18] for the sphere shape. Starting from Laplace's equation, analytical expressions were obtained in the framework of the quasi-static approximation, for simple geometrical shapes, such as spheres and ellipsoids. The dipolar

polarizabilities along the semi-major axis (x-axis, y-axis) and semi-minor axis (z-axis) of the prolate spheroids are different. When the incident light is along the z-axis, the applied electric field is polarized in parallel to the disk (x-y plane), the corresponding polarizabilities are then given by^[18].

$$\alpha_i = \frac{\epsilon_m}{L_i^2} \frac{\epsilon_2}{\left(\epsilon_1 + \frac{1-L_i}{L_i} \epsilon_m \right)^2 + \epsilon_2^2} \quad (7)$$

where the geometrical factors L_i ($i = x, y, z$ are the Cartesian directions) are given by $L_x + L_y + L_z = 1$, and $L_x = L_y$. Here, L_z writes, in term of the semi-major axis, as follows,

$$L_z = \frac{1-e_x^2}{e_x^2} \left[-1 + \frac{1}{2e_x} \ln \left(\frac{1+2e_x}{1-e_x} \right) \right] \quad (8)$$

$$e_x^2 = 1 - \eta^2 \quad (9)$$

$$\eta = a/b \quad (10)$$

where η and e_x represent the aspect ratio and the eccentricity of the ellipsoid, respectively. Combining eq. (3) and (7) yields the Gans Formulae^[18].

$$\sigma_{ext}^i = \frac{k V_p \epsilon_m^{3/2}}{L_i^2} \frac{\epsilon_2}{\left(\epsilon_1 + \frac{1-L_i}{L_i} \epsilon_m \right)^2 + \epsilon_2^2} \quad (11)$$

This relationship describes the extinction cross-section of the prolate inclusion, in the quasi-static limit, and it is very easy to find the other optical cross-sections. We also point out that the above relation is valid only for monodisperse inclusions and weak fractions. When the distance between particles becomes weak, however, this will have significant impact on their plasmonic behaviors. In fact, this is caused by the electromagnetic field coupling^[20]. In these conditions, the analytical theory should be modified for ellipsoid shape.

Dielectric dispersion of gold

Notice that the optical constants of the metal depend on the photon energy (or light wave-length λ). This optical response is generally related to the dielectric dispersion. We recall that the dielectric function was first computed using the Drude model^[21], because of its simplicity. It describes the metal confinement and the surface effects in a phenomenological damping constant.

Therefore, this theory considers only free electrons

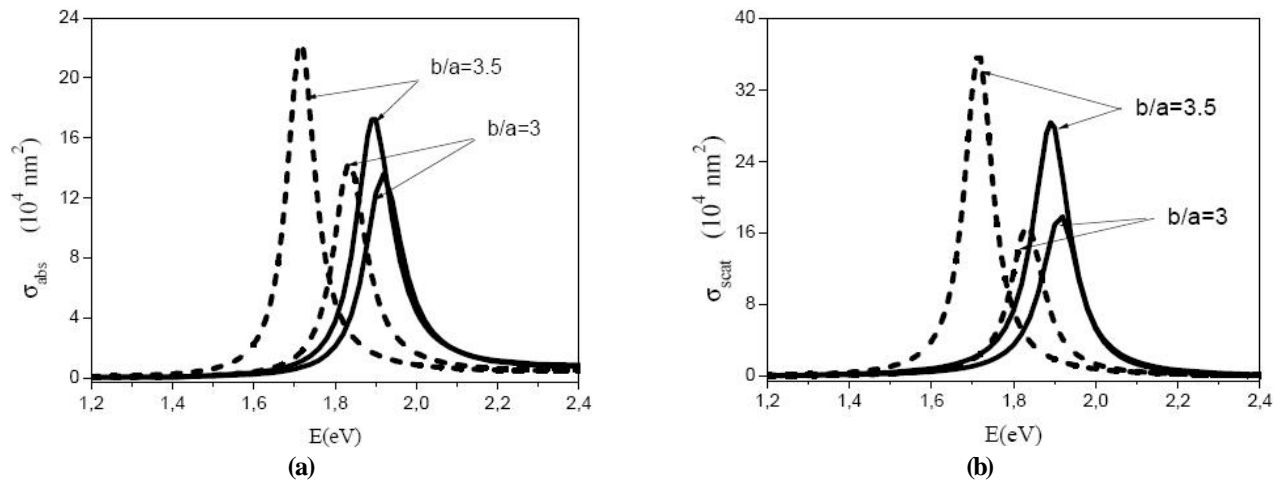


Figure 5 : Comparison between the absorption (a) and the diffusion (b) cross-sections of the gold prolate (dashed line) and the cylinder (solid line), for $b/a=3$ and 3.5 . The numerical parameters chosen are as follows: $f=0.1$ and $\epsilon_m=1.77$

contribution in metals. This means that the response to the electromagnetic field is mainly due to the transitions of the electrons in the conduction band, i.e. intraband transitions.

Furthermore, in order to improve this model, we have used the so-called Drude-Lorentz with two-critical points (DCP) model^[22] which reproduces the basic optical properties of metals. The virtue of such an extended model is that, it describes correctly the gold permittivity in a wide photonic energy band.

Figure 1 depicts the gold dispersion function upon the photon energy (electron-Volt), described within the DCP model and classical Drude theory. A comparison with measured data of Johnson & Christy^[23] is made.

There has been a growing interest to the description of metal permittivities by means of analytical models, and the DCP model gives a very good agreement with experimental data in the large band of wavelengths.

In the following section, we shall present the basic equations and draw the numerical approach enabling us to comprehend the optical properties of the anisotropic nanogolds clusters.

Numerical computation

The effective permittivity is determined for a matrix dielectric with inclusions, for various shapes and volume fractions of particles. Consider a composite for which the host material has a dielectric constant ϵ_m . The displacement field is then given by,

$$\vec{D} = \epsilon_0 \epsilon_m \vec{E} + \vec{P} \quad (12)$$

The effective permittivity of the inhomogeneous ma-

terial is then defined as

$$\vec{D} = \epsilon_0 \epsilon_{\text{eff}} \vec{E} \quad (13)$$

Using eq. (12) and (13) yields

$$\epsilon_0 \epsilon_{\text{eff}} \vec{E} = \epsilon_0 \epsilon_m \vec{E} + \vec{P} \quad (14)$$

The effective permittivity needs to be calculated numerically for arbitrary particles shapes. This is done starting from a resolution of Laplace's equation, using FEM for fixed nanogolds shape. FEM allows the determination of the electric field and potential distributions knowing both physical properties of material and boundary conditions.

To describe the FEM formalism, we consider a spatial domain, Ω , with a charge density equal to zero. We assume that the composite is non-magnetic and the frequency is low enough, so-that the interaction between the magnetic and electric fields can be neglected. In this case, the Laplace's equation reads

$$\vec{\nabla} \cdot (\epsilon(\mathbf{r}) \vec{\nabla} V(\mathbf{r})) = 0 \quad (15)$$

Here, $\epsilon(\mathbf{r})$ accounts for the local permittivity and $V(\mathbf{r})$ for the electrostatic potential. Taking into account the symmetry and periodicity properties, the geometry of the medium reduces to a unit cell. The interior volume is enclosed by four side surfaces, a top surface and a bottom surface. It may contain arbitrary dielectric matrix and metal inclusion, where L_1, L_2 and L_3 are lengths in the x, y and z-directions, respectively.

The problem consists to solve differential equation, together with the boundary conditions

Full Paper

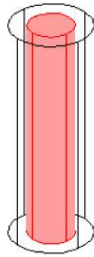


Figure 6 : Configuration of metallic cylinder inclusion with shell

$$\mathbf{V}(\mathbf{r}) = \mathbf{V}_1 = \mathbf{E}_0 L^3 (\text{on top surface}) \quad (16)$$

$$\mathbf{V}(\mathbf{r}) = \mathbf{V}_2 = 0 (\text{on bottom surface}) \quad (17)$$

where E_0 is the amplitude of the applied field. The elimination of fringing effects also has to be satisfied

$$\vec{\mathbf{n}} \times \vec{\nabla} \mathbf{V} = \mathbf{0} (\text{on sides}) \quad (18)$$

Here, $\vec{\mathbf{n}}$ is the normal vector to the considered surface.

The FEM's implementation consists in dividing the domain Ω into tetrahedral finite elements, and for each element. The potential and its normal derivative in this space can be approximated inside each element using interpolating functions^[15]. By solving the matrix equations resulting from the discretization procedure, we obtained electrical field and potential distributions on each node of the mesh.

Based on this potential distribution and its normal derivative, we compute both electrostatic stored energy and dielectric loss on each tetrahedral element of the computational mesh. The electrostatic energy can be evaluated as,

$$\mathbf{W}_e^k = \frac{1}{2} \iiint \varepsilon_k'(\mathbf{x}, \mathbf{y}, \mathbf{z}) \left(\left(\frac{\partial \mathbf{V}}{\partial \mathbf{x}} \right)^2 + \left(\frac{\partial \mathbf{V}}{\partial \mathbf{y}} \right)^2 + \left(\frac{\partial \mathbf{V}}{\partial \mathbf{z}} \right)^2 \right) d\mathbf{v}_k \quad (19)$$

and energy loss as

$$\mathbf{P}_d^k = \frac{1}{2} \iiint \omega \varepsilon_k''(\mathbf{x}, \mathbf{y}, \mathbf{z}) \left(\left(\frac{\partial \mathbf{V}}{\partial \mathbf{x}} \right)^2 + \left(\frac{\partial \mathbf{V}}{\partial \mathbf{y}} \right)^2 + \left(\frac{\partial \mathbf{V}}{\partial \mathbf{z}} \right)^2 \right) d\mathbf{v}_k \quad (20)$$

where ε_k and v_k represent the permittivity and the volume of the k th tetrahedral element, respectively, and ω is the frequency of the applied field. The components of the composite are described through their complex permittivity $\varepsilon_k = \varepsilon_k' + i\varepsilon_k''$. Therefore, the total energy, W_e , and losses in the entire composite, P_d , can be found summing over the total number of elements of mesh.

As already mentioned, to compute the quantities

W_e and P_d , we assume that the composite material is embedded in a plane capacitor. This procedure allows us to determine the effective permittivity in a direction parallel to the applied electric field. Thus, from the capacitor electrostatic energy expression, we deduce the effective complex permittivity. The real part, $\varepsilon_{\text{eff}}'$, and imaginary one, $\varepsilon_{\text{eff}}''$, are given by,

$$\mathbf{W}_e = \frac{1}{2} \varepsilon_{\text{eff}}' \frac{\mathbf{S}}{L_3} (\mathbf{V}_2 - \mathbf{V}_1)^2 \quad (21)$$

$$\mathbf{P}_e = \frac{1}{2} \varepsilon_{\text{eff}}'' \omega \frac{\mathbf{S}}{L_3} (\mathbf{V}_2 - \mathbf{V}_1)^2 \quad (22)$$

Here, $\mathbf{S} = L_1 \times L_2$ is the surface of in-depth.

More details of FEM applications to composite systems can be found in Refs.^[24-29].

The computation of the effective dielectric function of the composite, based upon the FEM (Eq. (21) and (22)), allows us to have access to the polarization vector using the eq. (14). The polarizability is calculated numerically using eq. (1) and (2), and the several cross-sections are given by eq. (3-5).

RESULTS AND DISCUSSION

We emphasize that several parameters can affect the optical resonance. These are absorption σ_{abs} and scattering cross-section σ_{scat} , with respect to the photon energy, the particle volume fraction, their shape and the shell (if it exists) surrounding them. Our aim is to quantify the effects of the volume fraction and shell around the inclusion.

For a comparison between numerical calculations by FEM and Gans formula, we first consider gold spheroids and excite the longitudinal plasmon resonance (LSP). In this calculation, the minor axis of gold prolate is kept constant and equal to 20nm, whereas, the dielectric constant of the matrix is 2.25.

Figure 2 and 3 illustrate the variations of the absorption and scattering cross-section for prolate shape, upon photon energy, which are calculated by FEM for $f=0.1$ and several values of η . In these figures, the analytical results are also represented. We observe that, for a diameter equal to 20nm, the absorption is greater than the scattering. In addition, these curves show that, when $f=0.1$, the optical resonance is produced around a photon energy equal to 1.9eV ($\lambda=650\text{nm}$) for $\eta=2.5$

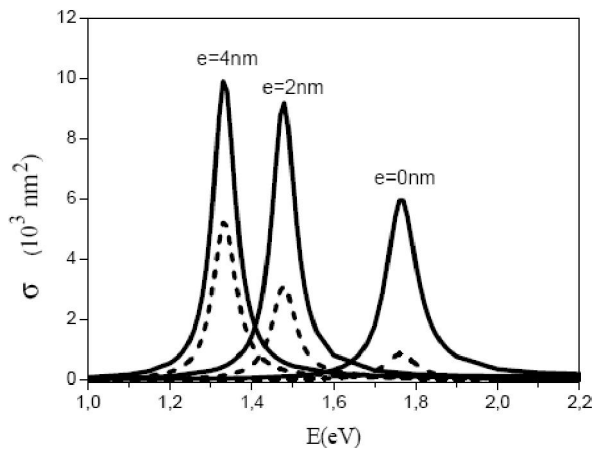


Figure 7 : Effect of the shell on the optical proprieties of a gold cylinder inclusion, for L mode and several shell depths ($e=0\text{nm}$, $e=2\text{nm}$ and $e=4\text{nm}$), by FEM simulation. The solid line represents the absorption, whereas the dashed one corresponds to the diffusion. The curves are drawn choosing: $2a=10\text{nm}$, $2b=50\text{nm}$, $f=0.1$, $\epsilon_m=1.77$ and $\epsilon_s=2.5$

and to 1.6eV ($\lambda=770\text{nm}$), if $\eta=3.5$. We observe a significant red shift in frequencies, with the increasing of the aspect ratio. A good agreement between FEM calculations and analytical results, corresponding to a filling factor $f=0.1$, is observed, especially when the anisotropy is not strong.

The volume fraction can be increased with the size of inclusions or their number density. In our case, we chose to keep constant the dimensions ($2a=40\text{nm}$ and $2b=80\text{nm}$) of inclusion and to decrease the volume of the matrix in the unit cell, such a way f is equal to 0.3 . The optical cross-sections are reported in figure 4.

The discrepancy, observed between numerical and analytical results, is due to the fact that Gans formula is valid only for weak inclusion volume fractions, i.e. for dispersed particles. It is worthwhile to point out that the fraction $f=0.1$ often corresponds to the case of isolated particles without interaction. Therefore, our approach provides an appropriate tool for the description of the optical properties of nanoparticles even if their density is strong.

Here, we focus our attention on the comparison between the two shapes: cylinder and spheroid. We consider a cylinder of diameter $2a$ and height $2b$. The minor and the major axis of the prolate inclusion are chosen equals to the diameter and the height of the cylinder, respectively, in order to have the same aspect ratio. We report FEM results for the absorption (Fig-

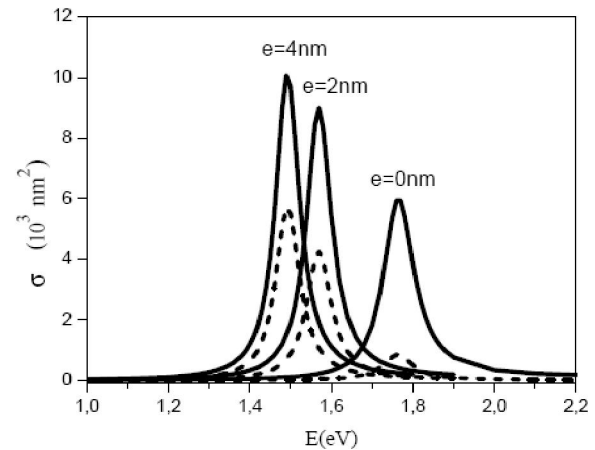


Figure 8 : Effect of the shell on the optical proprieties of a gold cylinder inclusion, for L mode and several shell depths ($e=0\text{nm}$, $e=2\text{nm}$ and $e=4\text{nm}$), by FEM simulation. The solid line represents the absorption, whereas the dashed one corresponds to the diffusion. The curves are drawn choosing: $2a=10\text{nm}$, $2b=50\text{nm}$, $f=0.1$, $\epsilon_m=1.77$ and $\epsilon_s=1$

ure 5a) and scattering cross-sections (Figure 5b) of a cylinder and a prolate inclusion, for two values of aspect ratios, and $2a$ is fixed to 40nm . For this diameter, the scattering increases and it is slightly greater than the absorption. When $b/a=3$, we observe that the cylinder and the prolate have the same absorption and scattering sections, but there is some shift in frequency between them. An increase in the aspect ratio implies a discrepancy in the frequencies and the amplitudes between the two considered shapes. We remark that the frequency shift is more pronounced when the shape is prolate.

These curves imply that there exist two competing key factors, a weighting factor assigned to the shape parameter and a dielectric function of the metal particle. This means that, for the prolate and cylinder nanoparticles, even if they have the same aspect ratio, their effect is certainly different depending on their exact geometry. In our case, the ellipsoid geometry has more significant positive contribution from the shape factor for the enhancement of absorbing and scattering efficiencies.

The FEM modeling is very versatile to study the effect of a shell surrounding the metal inclusion, where it represents the vacuum, a material like polymer or silica, having a permittivity ϵ_s and a depth noted e (Figure 6). In our calculations, the filling factor is relative to the both metal inclusion and the shell and is kept con-

Full Paper

stant. We also keep the dimensions of the gold cylinder constant, but we increase the depth of the shell; this means that the aspect ratio decreases.

We report numerical results of the optical cross-sections in figure 7, for the situation where the permittivity of the host matrix and the shell are 1.77 and 2.5, respectively. Since the absorption is greater than the scattering, we have multiplied the scattering cross-section by a 3-factor. These curves show that, in despite that the aspect ratio decreases and the metal volume is kept constant, the LSP is shifted toward the infrared frequencies in a manner very pronounced. When the shell's depth is equal to 4nm, a relative wavelength shift of value 0.346 occurs for $\epsilon_s=2.5$, and takes the value 0.166, for $\epsilon_s=1$ (Figure 8). This increase in the LSP, with decreasing shell-cylinder aspect ratio, is different from that predicted by Gans theory and FEM calculations, which state that, for an inclusion without shell and when its aspect ratio increases, the LSP occurs in the infrared frequencies.

In addition, it is also noted that both absorption and scattering cross-sections of the cylinder with a shell are greater than those of the same cylinder without shell. This dependence of the scattering and absorption properties of Au nanocylinder on their surrounding shell is worth investigation, because the use of the kind of metal inclusion for optical and biotechnological applications often requires that they are surrounding with various materials and biological molecules.

Concluding remarks

In this work, we have introduced a numerical modeling based on the Finite Element Method, in order to compute the optical absorption and scattering of gold anisotropic inclusions embedded in a dielectric medium. We have observed that the optical properties strongly depend on the shape and the inclusion volume fraction. A difference between spheroid and cylinder spectra is also shown. The results associated with nanocylinders (reported in literature), are treated as prolate spheroids in Gans theory, without taking account for the phase retardation and higher-order contributions. In this paper, however, they are exactly treated according to their size and shape in FEM calculations.

Our approach provides a large scope for the description of the optical properties of nanoparticles, even

if their density is strong. This numerical modeling allowed us to study the effect of the shell or the vacuum between the metal inclusion and the host matrix (this can occur when the metal grows in the anodic aluminum oxide matrix).

Finally, we emphasize that the numerical method, developed in this paper, can be extended to investigate the electromagnetic coupling between particles and its effect on the plasmonic behaviors.

ACKNOWLEDGEMENTS

One of us (A.R.S.) is much indebted to Professor M. Benhamou for fruitful and enlightening discussions.

REFERENCES

- [1] J.Zhu, J.J.Li, J.W.Zhao; *J.Matter.Sci.*, **43**, 5199 (2008).
- [2] K.S.Lee, M.El Sayed; *J.Phys.Chem.B*, **109**, 20331 (2005).
- [3] S.Link, M.B.Mohamed, M.A.El Sayed; *J.Phys.Chem.B*, **103**, 3073 (1999).
- [4] A.M.Gobin; *Nano.Lett.*, **7**, 1929 (2007).
- [5] A.N.Volkov, C.Sevilla, L.V.Zhigilei; *App.Surface Sci.*, **253**, 6394 (2007).
- [6] J.L.West, N.J.Hallas, L.R.Hirsch; *United State Patent*, 6530944 (2003).
- [7] L.R.Hirsch; *Ann.Biomedical Eng.*, **34**, 15 (2006).
- [8] J.C.Maxwell Garnett; *Phil.Trans.R.Soc.Lond.*, **203**, 385 (1904).
- [9] G.A.D.Bruggeman; *Ann.Phys.(Leipzig)*, **24**, 636 (1935).
- [10] A.K.Sarychev, V.M.Shalaev; 'Electrodynamics of Metamaterials', World Scientific, Singapore, (2007).
- [11] G.Mie; *Ann.Phys.*, **25**, 377 (1908).
- [12] M.I.Mishchenko, J.W.Hovenier, L.D.Travis, Eds.; 'Light Scattering by Nonspherical Particles', Academic, San Diego, Calif., (2000).
- [13] K.S.Lee, M.A.El-Sayed; *J.Phys.Chem.B*, **109**, 20331 (2005).
- [14] A.Mejdoubi, C.Brosseau; *J.Appl.Phys.*, **99**, 063502 (2006).
- [15] J.N. Reddy; 'Introduction to the Finite Element Method', Mc Graw Hill Inc., (1993).
- [16] A.R.Senoudi, F.Lallam, A.Boussaid, M.Benhamou; *Inter.J.Acad.Research*, **2**, 70 (2010).
- [17] J.D.Jackson; 'Classical Electrodynamics', 3rd edition, John Wiley and Sons, (1999).

- [18] C.F.Bohren, D.R.Huffman; 'Absorption and Scattering of Light by Small Particles', Wiley Interscience, New York, (1983).
- [19] B.N.J.Persson; Surface Science, **281**, 153 (1993).
- [20] C.Rockstuhl, M.G.Salt, H.P.Herzig, J.Opt.Soc.Am.A, **21**, 1761 (2004).
- [21] A.Vial, T.Laroche; J.Phys.D: Appl.Phys., **40**, 7152 (2007).
- [22] A.Vial, T.Laroche; Appl.Phys.B, **93**, 139 (2008).
- [23] P.B.Johnson, R.W.Christy; Phys.Rev.B, **6**, 4370 (1972).
- [24] B.Sareni, L.Krahenbuhl, A.Beroual; J.Appl.Phys., **81**, 2375 (1997).
- [25] B.Sareni; J.Electr.Elsevier J., **40 & 41**, 489 (1997).
- [26] B.Sareni, L.Krahenbuhl, A.Beroual; J.Appl.Phys., **80**, 4560 (1996).
- [27] B.Sareni; Appl.Phys., **80**, 688 (1996).
- [28] E.Tuncer; Turk J.Phys., **27**, 121 (2003).
- [29] X.Zhao, Y.Wu, Z.Fan, F.Li, J.Applied Phys., **95**, 8110 (2004).